RESEARCH PAPER

Enhanced Deep Learning Approach for Autism Spectrum Disorder Detection Using MRI Images

Kurakula Naga Sandhya[1], Avani Anawardekar[2], Saritha P S[3], Revati Anawardekar[4], Dr. Surem Samuel S R[5] and Gokul A[6].

[1]Assistant Professor, Department of CSE-Data Science, VNR Vignana Jyothi Institute of Engineering and technology, Hyderabad,
[2]Avani Anawardekar, Assistant Professor, Department of Artificial Intelligence and Data Science, Marathwada Mitra Mandal's College of Engineering, Pune,
[3]Assistant Professor, Department of Artificial Intelligence and Data Science, Dhanalakshmi Srinivasan College of Engineering, Coimbatore,
[4]MBA, Management Development Institute, Gurgaon, MSc, Jain University, Bengaluru,
[5]Associate Professor, Department of Electronics and Communication Engineering, Kingston Engineering College, Vellore, suremsam.
[6]Assistant Professor, Department of Cyber Security, Paavai College of Engineering, Namakkal,
[1]nagasandhya1993@gmail.com, [2]avanianawardekar@mmcoe.edu.in, [3]sarithasaranya45@gmail.com, [4]revati.anawardekar@gmail.com, [5]engineering@kingston.ac.in and [6]gokuldominator@gmail.com
**** Corresponding author:** Kurakula Naga Sandhya*

Received: 24th April, 2026; Revised: 20th May 2026; Accepted: 30th June, 2026; Available Online: 10th July, 2026

ABSTRACT
Autism Spectrum Disorder (ASD) is a developmental condition that affects communication, social interaction, and behavior. Detecting ASD at an early stage is important because it can help improve treatment and support outcomes. Traditional diagnosis methods usually depend on behavioral observation, which can take time and may vary between specialists. This study proposes a deep learning-based system for automatic ASD detection using Magnetic Resonance Imaging (MRI) brain scans. MRI data from the Autism Brain Imaging Data Exchange dataset were processed using normalization, resizing, and slice extraction methods before training the model. An improved Recurrent Neural Network (RNN) with batch normalization and dropout layers was used to classify ASD and non-ASD subjects. Experimental results showed strong accuracy and good overall performance. The proposed system can help doctors by providing a faster and more objective tool for ASD screening and diagnosis.

Keywords: Autism Spectrum Disorder, MRI, Deep Learning, RNN, Medical Imaging, Artificial Intelligence

How to cite this article: Sandhya KN, Anawardekar A, Saritha PS, Anawardekar R, Samuel SRS, Gokul A, Enhanced Deep Learning Approach for Autism Spectrum Disorder Detection Using MRI Images Int J Drug Deliv Technol. 2026;16(6): 988-1007. DOI: 10.25258/ijddt.16.6.141
Source of support: Nil.
Conflict of interest: None

1. INTRODUCTION:

Inflammation serves a critical function in the body—it protects us from infection and helps tissues heal. However, when inflammation doesn't turn off or spirals out of control, it becomes destructive. This uncontrolled inflammatory state underlies major diseases consisting of rheumatoid arthritis (RA), inflammatory bowel disease (IBD), and neurodegenerative disorders. Understanding how to selectively dampen pathological inflammation while preserving its protective functions remains a significant therapeutic challenge. Collectively, chronic inflammatory diseases account for approximately 60% of global deaths (1,2). Current anti-inflammatory strategies, including NSAIDs, corticosteroids, and biologics such as IL-6 and TNF-α inhibitors, have transformed management of acute inflammation as well as autoimmune diseases. However, each class carries significant limitations that restrict long-term use. NSAIDs act primarily through cyclooxygenase (COX) inhibition and provide symptomatic relief, but are associated with gastrointestinal toxicity, renal impairment, and cardiovascular complications, particularly with long-term use (3). Corticosteroids, while highly effective, carry substantial long-term toxicity including osteoporosis, gastrointestinal ulceration, metabolic disturbances, immunosuppression, and avascular necrosis (4). Biologic therapies targeting TNF-α, IL-6, or JAK-STAT signalling demonstrate efficacy in only 40-60% of patients with RA and IBD, and their high cost and immunosuppressive effects limit accessibility and long-term safety. Importantly, these therapies typically target single inflammatory mediators, which may prove insufficient in diseases characterized by network-level dysregulation and pathway redundancy (5). The acute inflammatory response is essential for host defence and involves a coordinated network of cytokines,

**Author for Correspondence: Kurakula Naga Sandhya*

kinases, transcription factors, and immune effector cells. When this coordination is disrupted by environmental triggers, genetic predisposition, or persistent pathogenic stimuli, the resulting dysregulation involves multiple interconnected signalling pathways rather than isolated molecular defects (6,7). This single-target paradigm often fails to address the complexity of inflammatory networks, contributing to suboptimal response rates and treatment resistance.

A shift in pharmacological research toward isolated bioactive constituents derived from medicinal plants has been driven by the growing interest in herbal medicine (8). A variety of plant-derived secondary metabolites, including polyphenols, terpenoids, and alkaloids, have been reported to strongly regulate inflammatory responses by modulating key signalling pathways that include JAK–STAT, MAPK, and NF-κB (9). Columbin, a primary constituent of Menispermaceae family such as *Tinospora* sp. and *Jateorhiza palmata,* has been reported as anti-inflammatory agent in various preliminary studies (10–12). It has been reported to inhibit cyclooxygenase (COX) enzymes, with stronger activity against COX-1 (≈64% inhibition at 100 μM) than COX-2 (≈19% at 100 μM) in in vitro studies(13). However, the molecular targets and network-level mechanisms underlying columbin's anti-inflammatory activity remains poorly characterized.

To explore the anti-inflammatory mechanisms of columbin, a comprehensive computational workflow incorporating network pharmacology, molecular docking, and external gene expression validation was implemented to characterize its target landscape and pathway associations. This systems-level approach provides comprehensive understanding of interaction landscape as well as biological relevance. These findings provide the first systematic characterization of columbin's multi-target anti-inflammatory mechanisms and establish a computational framework applicable to other phytochemical lead optimization efforts.

2. MATERIALS AND METHODS:

The complete workflow of the present study, including data acquisition, bioinformatics analyses, target identification, network construction, and validation procedures, is illustrated in Fig 1. The workflow contains target identification, network pharmacology analysis, molecular docking, validation, and ADMET prediction.

2.1. Identification of columbin and inflammation-related targets

PubChem was used to obtain chemical information of Columbin (PubChem ID: 188289)(14). SwissTargetPrediction (probability > 0.1), SuperPred (probability ≥ 50%), TargetNet (probability ≥ 0.5), and PharmMapper (normalized fit score ≥ 0.7) were used to predict potential protein targets with default or recommended thresholds(15–18). Targets predicted from different databases were integrated, and redundant entries were filtered out to obtain a curated, non-redundant list of unique targets. Further, to increase confidence, targets that were found to be predicted by at least two databases or confirmed by differential expression analysis was considered, while the targets with low confidence (predicted by only one database) were removed.

Parallelly, GeneCards (v5.26) and DisGeNET (v26.1) were used to obtain genes associated with "inflammation," "inflammatory response," and "chronic inflammation." GeneCards (relevance score ≥ 30) as well as DisGeNET (gene-disease association score ≥ 1) were used to extract inflammation-related genes(19,20). The microarray dataset GSE55235 was obtained from the Gene Expression Omnibus (GEO) repository for further analysis (21). The dataset consist of synovial tissue samples of rheumatoid arthritis patients and healthy controls. Raw microarray expression data generated using the Affymetrix Human Genome U133 Plus 2.0 platform were preprocessed through background adjustment and normalization procedures utilizing the Robust Multi-array Average (RMA) algorithm to minimize technical variability and improve data comparability. Differential expression analysis was conducted using the limma package, which applies an empirical Bayes framework to improve the estimation of gene-wise variances. To control for multiple testing and reduce the likelihood of false-positive findings, the resulting p-values were adjusted using the Benjamini–Hochberg false discovery rate (FDR) correction method. Differentially expressed genes meeting the thresholds of $|\log_2 FC| > 1$ and FDR < 0.05 were deemed statistically significant and were further utilized for the screening and identification of candidate targets associated with columbin (21). These genes were further visualised through volcano plot and integrated with disease related genes.

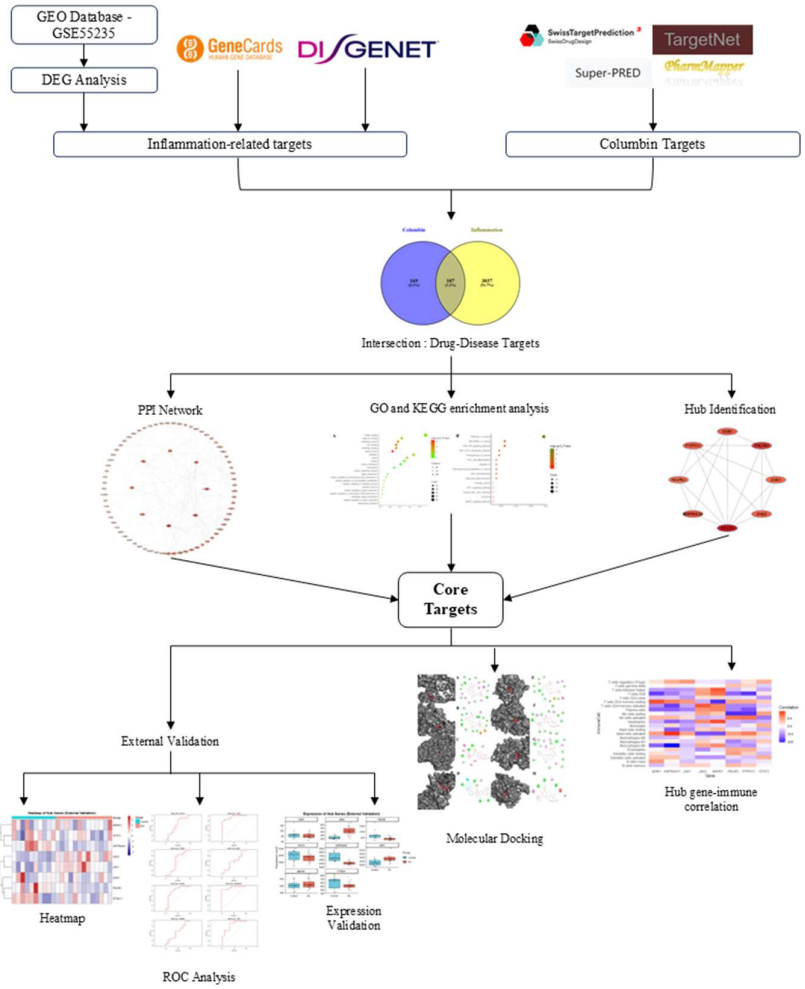

Fig. 1: --- Systematic workflow illustrating the stepwise methodology of a network pharmacology study.

2.2. Venn diagram and construction of PPI network

Columbin targets (Set A) were predicted from four servers (SwissTargetPrediction, TargetNet, PharmMapper and SuperPred), and these were combined to create a unique set (n = 169). A list of genes associated with inflammation (Set B) was created by integrating the GeneCards and DisGeNET databases. Furthermore, using the cut-off points $|\log_2 FC|>1$ and FDR<0.05, the significantly differentially expressed genes (Set C) in the dataset GSE55235 were identified. The common elements present in the predicted columbin targets (Set A) and combined pool of inflammation-associated and differentially expressed genes (Sets B and C) were subsequently determined using the program Venny (v2.1) to identify candidate therapeutic targets. Overlapping genes were deemed as possible mediators of the therapeutic effects of columbin (22).

PPI networks had been generated with the STRING database. To ensure reliable predictions while retaining network connectedness, a high-confidence interaction score threshold of ≥ 0.700 was used (23). All evidence sources were considered with the default integrated scoring system of STRINGA comprehensive interaction network of the candidate targets was generated to characterize their functional relationships, with network organization and visualization performed using Cytoscape software (v3.10.4). The CytoHubba plugin systematically identified hub genes within the static network by implementing five centrality-based algorithms, namely Degree, Betweenness, Maximal Clique Centrality (MCC), Closeness and Density of Maximum Neighborhood Component (DMNC). The ten highest-ranked genes from each algorithm were extracted, and those consistently identified by a minimum of three out of the five methods were defined as hub genes. As a consequence, 8 hub genes were identified (24).

2.3. Gene Ontology and Pathway Enrichment Analysis

Functional enrichment analysis was performed by employing the DAVID (Database for Annotation, Visualization, and Integrated Discovery, 2025) platform to identify and interpret biological functions and pathways corresponding to the

gene collection (25). Functional enrichment analysis was conducted to investigate the biological significance of the identified gene set. Gene Ontology (GO) categories, including Biological Process, Molecular Function, and Cellular Component, as well as KEGG pathways, were analyzed. Multiple testing correction was performed using the Benjamini–Hochberg method, and enriched terms with FDR (false discovery rate) < 0.05 were deemed statistically significant.

2.4. Ligand and protein preparation

Three-dimensional crystallographic structures of the selected target proteins were retrieved from the RCSB Protein Data Bank for subsequent structural and molecular analyses. Structures co-crystallized along with the ligand of resolution ≤3.0 Å were selected to establish the binding location and quality of the structure utilized for molecular docking. Prior to docking, the target protein structures were prepared using AutoDockTools by removing crystallographic water molecules, incorporating polar hydrogen atoms, and applying Gasteiger charges. The molecular structure of columbin was retrieved from PubChem and transformed into Protein Data Bank (PDB) format for use in subsequent in silico studies (26). PIK3R1 was identified as a hub gene through network analysis, however, PIK3R1 (p85α regulatory subunit) functions as part of a heterodimeric complex with PIK3CA (p110α catalytic subunit) to form functional class I PI3K. Since PIK3R1 lacks intrinsic catalytic activity and there are no experimental data demonstrating PIK3R1 to be a direct target of small molecule inhibitors, molecular docking was performed with the heterodimer PIK3CA-PIK3R1 structure (PDB: 7PG6) to evaluate columbin binding to the biologically relevant PI3K complex. This approach is consistent with established PI3K inhibitor screening methodologies, where compounds are evaluated against the catalytic domain within the functional heterodimer (27).

2.5. Molecular docking-based target interaction study

Molecular docking studies were conducted using AutoDock Vina to investigate the binding affinity and interaction patterns between the selected ligand and the target protein, enabling assessment of their potential molecular recognition and stability within the binding site (28). The docking grid box was defined based on the centroid of the co-crystallized ligand and was configured to fully cover the active binding site, with additional spacing included to ensure adequate conformational sampling within the entire binding pocket (29). Grid box was centred on co-crystallized ligand centroid with dimensions of 20×20×20 Å binding pocket. An exhaustiveness value of 32 was employed to enhance the accuracy and reliability of ligand conformational sampling within the binding site. The most favorable binding posture was chosen based on the smallest binding free energy, with the lowest-energy conformation being regarded the best and most stable interaction between the ligand and target protein. The interactions were analysed through PyMOL and Discovery Studio (30,31). By redocking the co-crystallized ligand and computing RMSD values, the docking process was validated. Binding energy was cross validated using SwissDock (32).

2.6. Immune cell infiltration analysis

The immune landscape of synovial tissue samples was characterized using the CIBERSORT deconvolution method and the LM22 reference signature matrix, allowing quantification of the relative abundance of 22 immune cell populations from gene expression profiles (33). On the discovery dataset (GSE55235), we performed CIBERSORT with 1,000 permutations and kept those samples that showed reliable deconvolution ($p<0.05$). We concentrated our correlation analysis on four immune cell subsets with known roles in the pathophysiology of rheumatoid arthritis: neutrophils, macrophages, dendritic cells, and natural killer cells in order to prevent inflating false positives through excessive multiple testing. Testing all 22 cell types against 8 hub genes would have yielded 176 correlations, most of which would lack biological relevance. Correlation values with $|r|>0.45$ and $p<0.05$ were illustrated in a heatmap utilizing the corrplot R tool.

2.7. External Transcriptomics Validation

2.7.1. Gene expression analysis

To validate the findings, an independent external cohort was used, with the GSE55457 dataset retrieved to verify the expression patterns of the identified hub genes (21). It consisted of RA patients (n=13) and control (n=10), containing synovial tissues. Inter-cohort variability was minimized by applying appropriate normalization and batch-effect correction methods. Gene expression differences between groups were identified using the limma package in R, with p-values corrected for multiple testing using the Benjamini–Hochberg method to control the false discovery rate (34). Eight hub genes were selected and their expression across the samples was measured to assess their differential expression between RA and controls. Genes with adjusted $p < 0.05$ and similar expression patterns as the discovery group were validated. Plots were generated using ggplot2 and pheatmap.

2.7.2. ROC curve analysis:

The core targets' diagnostic performance was assessed using the pROC function in R, with independent dataset validation with GSE55457 (21). The expression levels of each hub gene were employed as predictor variables, with disease status (rheumatoid arthritis vs control) as the binary outcome. The area under the receiver operating characteristic curve (AUC)

and its corresponding 95% confidence intervals were estimated using 2,000 stratified bootstrap iterations. Acceptable diagnostic performance was defined as an AUC value ≥ 0.70.

2.8. ADMET Analysis

Pharmacokinetics and toxicity of columbin were predicted with several in silico ADMET prediction tools. Physicochemical properties were predicted using SwissADME and permeability, metabolism and toxicity endpoints were predicted using pkCSM (35,36). Additional toxicity parameters, including hepatotoxicity, drug-induced liver injury (DILI), and carcinogenicity were predicted using ProTox 3.0 (37).

3. RESULT:

3.1. Identification of Columbin and Disease Targets

An overall of 169 possible columbin targets were identified from SwissTargetPrediction, PharmMapper, TargetNet and SuperPred. Parallely, 3,037 inflammation-related genes were identified from GSE55235, DisGeNET, and GeneCards. GEO dataset was used to analyze differential expression genes. A volcano plot was used to identify genes that were significantly up- or down-regulated (fig. 2A).

Venn diagram analysis identified 107 genes at the intersection of columbin predicted targets (n=169) and inflammation-related genes (n=3,037), representing 63.3% of columbin targets with established inflammatory associations (fig. 2B). These 107 genes were subjected to PPI network analysis.

3.2. PPI Network and Hub Gene Identification

Ninety (84.1%) of the discovered genes were successfully mapped in the STRING database, creating a network of related protein–protein interactions. The remaining 17 genes showed no interactions at the selected high-confidence threshold (≥0.7) and were therefore excluded from further network analysis. The Cytoscape was used to visualize (fig. 3A,3B) and the structure was examined. The top regulation genes of PPI network were selected using 4 algorithms from plugin of CytoHubba to analyse their topological structure. Hub gene identification using CytoHubba revealed 8 core targets that ranked in the top 10 by all four centrality measures (Degree, Betweenness, Closeness, and MCC). These genes (ESR1, JAK2, PIK3R1, STAT3, HSP90AA1,

JAK1, MAPK1, and PTPN11) were selected for molecular docking and validation (fig. 3B).

3.3. Functional Enrichment Analysis

According to DAVID functional enrichment study on the overlapped genes, signal transduction, transcription, and cell proliferation are the main biological processes that are enriched (Figure 4A,4B). Gene Ontology (GO) analysis revealed 69 significantly enriched biological processes (FDR < 0.05) associated with response to stimuli and cell proliferation. The top terms include “signal transduction” (n = 19 genes) followed by “positive regulation of transcription by RNA polymerase II” (n = 17 genes) (Figure 4A). Analysis of cellular components (CC) showed significant enrichment in cytoplasm (47 genes) and cytosol (40 genes), which is in line with the role of these targets in intracellular signalling pathways. Molecular function (MF) analysis identified a high enrichment in protein binding (60 genes) as well as metal ion binding (34 genes).

KEGG pathway enrichment analysis revealed 57 significantly enriched pathways (FDR < 5E-02) that were mainly related to cancer processes and signal transduction. The pathways with the most significant enrichment were "Pathways in cancer" (n = 26 genes), "MicroRNAs in cancer" (n = 12 genes) and the "PI3K-Akt signalling pathway" (n = 12 genes) (Figure 4B). These findings show the role of the identified targets in cancer regulation and essential signal transduction pathways.

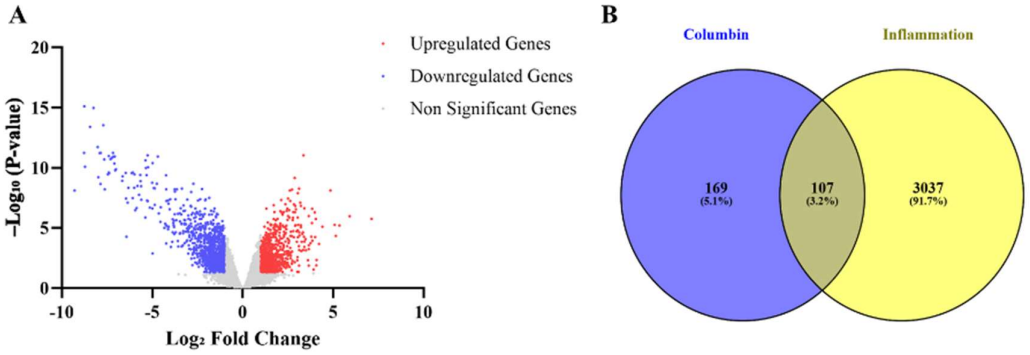

Fig. 2: --- Network construction and gene identification. (A) Volcano plot illustrating differentially expressed genes (DEGs) derived from GSE55235 dataset. (B) Venn diagram showing the intersection among columbin-associated targets and genes implicated in inflammation.

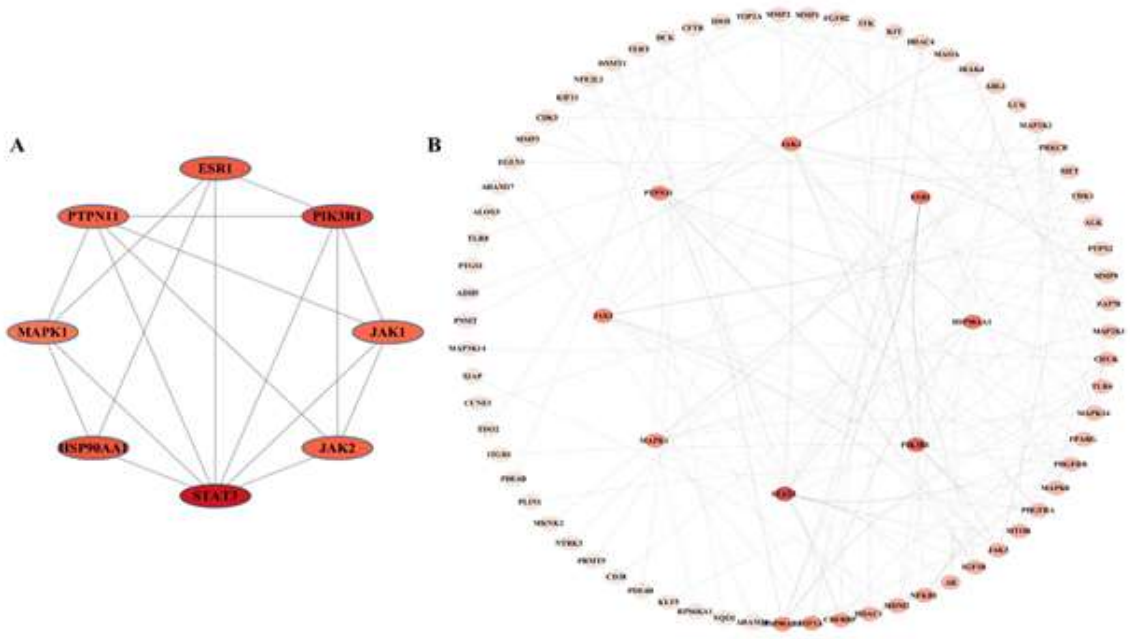

Fig. 3: --- (A) PPI network generated from the intersecting targets; (B) Hub genes identified through CytoHubba-based network analysis.

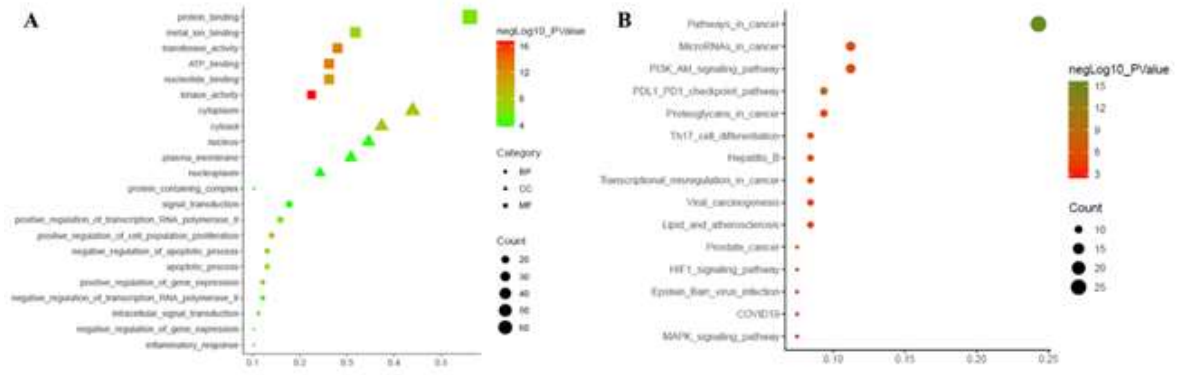

Fig. 4: --- (A) GO enrichment of common genes across BP, CC, and MF categories. (B) KEGG pathway enrichment of shared targets.

3.4. Molecular Docking Analysis

Molecular docking analysis revealed favorable binding of columbin with all selected targets. Binding energies obtained from AutoDock Vina ranged from −6.9 to −8.6 kcal/mol, while SwissDock scores varied between −6.4 and −7.7 kcal/mol. Among the targets, ESR1, HSP90AA1, and MAPK1 exhibited the strongest binding affinities (Table 1). When compared with native ligands it is seen that even though the binding energies are slightly lower, columbin still showed consistently binding against the active binding site. On detailed examination of the interaction of columbin with targets it was seen that columbin showed multiple hydrogen bonds with crucial active site residues (fig. 5). The length of hydrogen bond interactions was seen to be around 1.87-3.42 Å. The RMSD values of all docked complexes were below 2 Å demonstrating that columbin forms stable binding interactions with various inflammation-related targets.

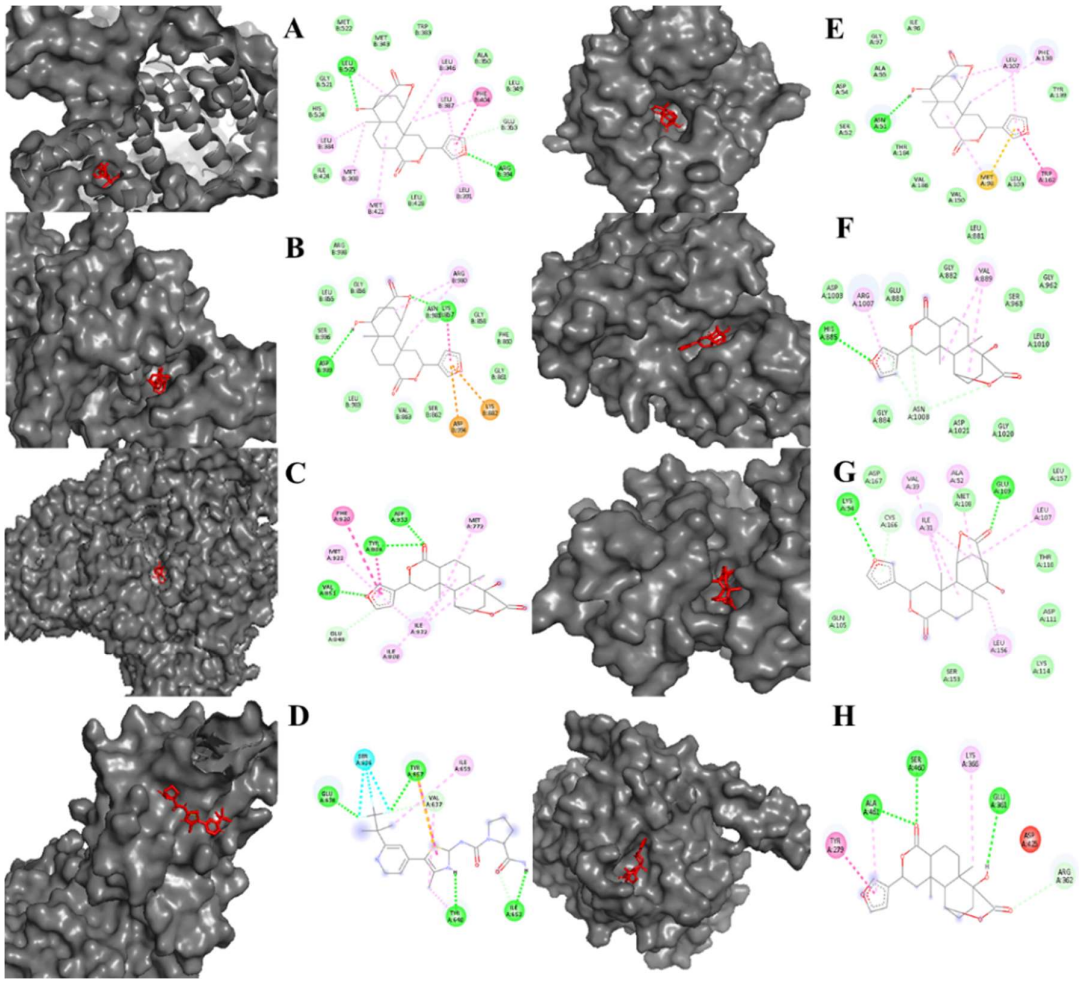

Fig. 5: --- 3D molecular docking models illustrating ligand binding within protein active sites: A–ESR1, B–JAK2, C–PIK3CA–PIK3R1, D–STAT3, E–HSP90AA1, F–JAK1, G–MAPK1, and H–PTPN11.

Table 1 – Molecular docking results of columbin and native ligand with core targets.

Protein	PDB IDs	Autodock ΔG (kcal/mol)	SwissDock ΔG (kcal/mol)	Native Ligand	Native ligand binding energy (kcal/mol)	Residues participating in H-bond formation	H-bond length (Å)	RMSD
ESR1	1A52	-8.615	-6.7564	EST	-10.75	ARG394, LEU525, GLU353	2.63, 3.09, 2.92	0.469
JAK2	2B7A	-7.306	-6.7427	IZA	-11.11	ASP939, LYS857	2.64, 2.22	0.893
PIK3CA-PIK3R1	7PG6	-7.892	-6.9448	1LT	-10.02	TYR836, VAL851, ASP933, GLU849	2.46, 1.94, 2.25, 3.29	1.65
STAT3	6NJS	-7.074	-7.663	KQV	-7.221	ILE653, TYR640, GLU638, TYR657, VAL637	1.87, 1.92, 2.83, 2.63, 2.79	1.851
HSP90AA1	3O0I	-8.4	-7.2709	P54	-9.564	ASN51	2.25	1.774
JAK1	3EYG	-6.957	-6.4467	MI1	-7.86	HIS885, ASN1008	2.94, 3.42	0.402
MAPK1	1WZY	-8.3	-7.6822	F29	-8.243	LYS54, GLU109,	2.86, 1.96,	1.25
PTPN11	3B7O	-8.072	-7.7772	MLT	-4.814	GLU361, SER460, ALA461, ARG362	3.01, 3.02, 2.81, 3.35	1.583

3.6. Immune cell infiltration analysis

The relationship between gene expression levels and immune cell infiltration was analyzed to elucidate the potential role of hub genes in modulating immune responses in rheumatoid arthritis. To reduce potential false-positive inflation from testing all 22 immune cell types, we focused on biologically relevant immune populations known to contribute to rheumatoid arthritis, namely macrophages, neutrophils, natural killer (NK) cells, as well as dendritic cells. Several hub genes showed strong associations with specific immune populations (fig. 6MAPK1 is also strongly correlated to neutrophils ($r=0.69$, $p<0.001$), therefore indicating that MAPK1 is involved in neutrophil activation and chemotaxis. It was also positively correlated to neutrophils ($r=0.49$, $p=0.03$), confirming JAK-STAT pathway activation in myeloid cell activities (fig. 6). However, HSP90AA1 was negatively correlated to neutrophils ($r=-0.55$, $p=0.01$), which suggests it can attenuate inflammation rather than promote it. The most intense negative correlations were with resting natural killer (NK) cells in which PIK3R1 ($r=-0.74$, $p<0.001$) and PTPN11 ($r=-0.72$, $p<0.001$) strongly correlate inversely, demonstrating either activation of NK cells or shift in its cellular distribution under the conditions of inflammation. There was little to no significant correlation with STAT3, ESR1 and JAK1 in these specified cell types, indicating its roles may be context-dependent or involving other non-tested immune populations. These patterns, combined, suggest that the hub genes interact with immune microenvironment differently: some positively promote neutrophils inflammation (MAPK1, JAK2), other possibly in activating innate immunity through NK cell pathway (PIK3R1, PTPN11). Therefore, columbin

potentially functions as a multi-target modulators of immune-inflammatory networks.

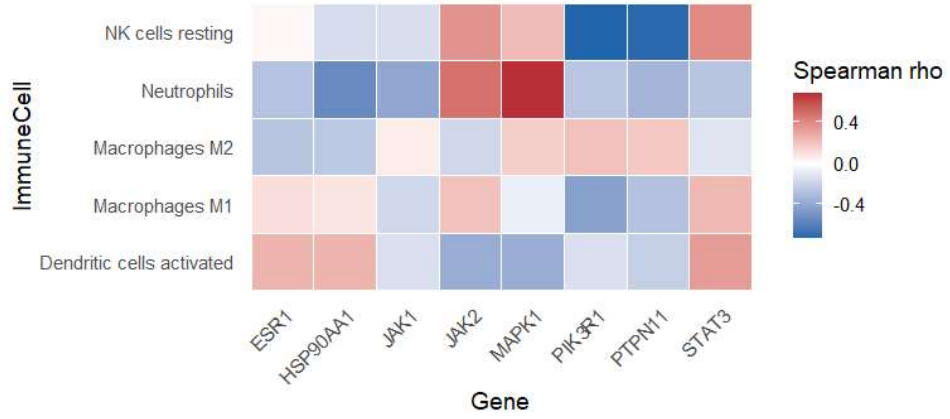

Fig. 6: --- CIBERSORT-based heatmap showing the relative proportions of immune cell infiltration across samples.

3.7. Transcriptomic Validation

3.7.1. Gene Expression Analysis

Two hub genes, JAK2 and HSP90AA1, displayed statistically significant differential expression in the independent GSE55457 cohort (13 RA, 10 controls) after multiple-testing correction (adj. P<0.05) (Fig. 7 A). Even with relatively small changes in expression magnitude (0.6- to 1.8-fold), hierarchical clustering on all 8 genes segregated samples according to disease state (Fig. 7 B). This suggests that a constellation of coherently varying genes, rather than an individual gene showing massive changes, distinguishes RA from control and is perhaps a hallmark of how columbin targets impact the condition. This supports the idea that columbin-treated genes function as control points rather than effector proteins exhibiting extremely altered expression levels. This observation is also consistent with the success shown by the ROC curve even with modest differential expression, indicating a consistent change in expression direction across multiple genes.

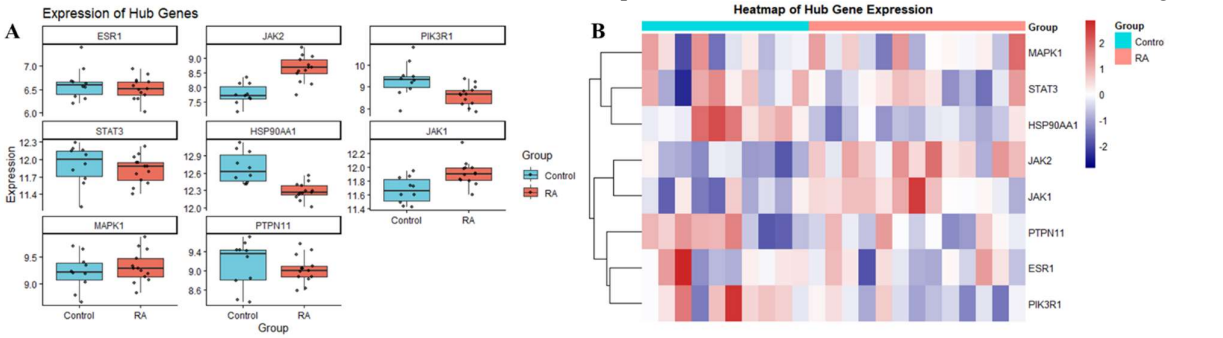

Fig. 7: ---(A) Boxplot showing differential gene expression in the GEO dataset between disease and control samples. (B) Heatmap of differentially expressed gene expression across GEO dataset samples.

3.7.2. ROC Curve Analysis

ROC curve analysis suggested that 5 of 8 hub genes had an AUC >0.70, indicating good to exceptional discriminating capacity between RA and control samples (fig. 8, Table 2). The high AUC values achieved by JAK1, JAK2, and HSP90AA1 illustrated a potential for these genes to be used as diagnostic biomarkers to discriminate RA from controls whereas ESR1, PTPN11 AND MAPK1 possesses a poor predictive value among all core target genes, suggesting that its role in inflammation may be more regulatory or context-dependent rather than consistently dysregulated across all RA patients.

Table 2 --- AUC values from ROC analysis representing the diagnostic performance of core targets.

Gene symbol	Expression Change (log_2FC)	Mean Expression Level	Moderated t Value	P.Value	adjusted p-value (adj.P.Val)	B Score	Expression Fold Change

JAK2	0.8593	8.2601	5.0034	4.23E-05	0.0053	2.1921	1.8142
JAK1	0.2468	11.8005	2.5915	1.61E-02	0.1073	-3.3007	1.1866
MAPK1	0.0914	9.2762	0.6668	5.11E-01	0.7281	-6.0362	1.0654
STAT3	-0.0804	11.8559	-0.6157	5.44E-01	0.7489	-6.0685	0.9458
PTPN11	-0.1022	9.0631	-0.6190	5.42E-01	0.7474	-6.0665	0.9316
ESR1	-0.1028	6.5653	-0.7868	4.39E-01	0.6741	-5.9506	0.9312
HSP90AA1	-0.4080	12.4630	-3.9637	5.86E-04	0.0186	-0.2642	0.7537
PIK3R1	-0.7334	8.9157	-2.8821	8.24E-03	0.0744	-2.7002	0.6015

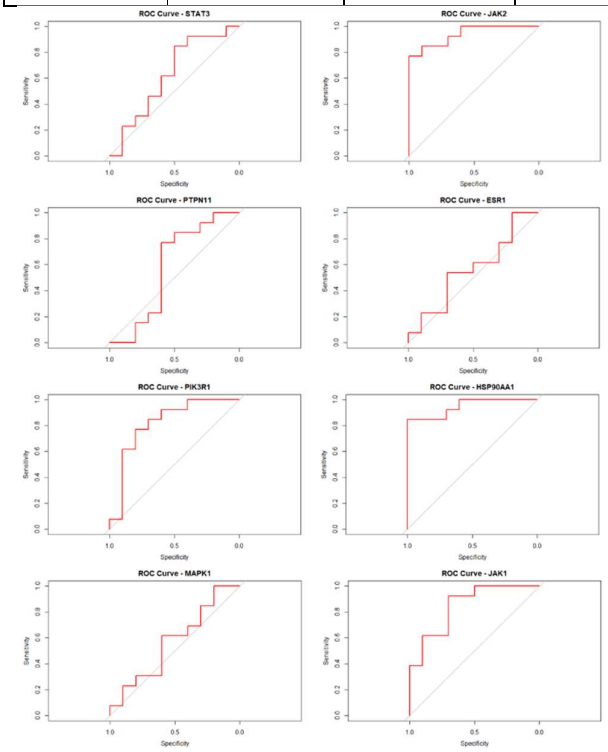

Fig. 8: --- ROC curves illustrating the diagnostic accuracy of key genes, along with their respective area under the curve (AUC) values.

3.7. ADMET Analysis

Columbin possessed good pharmacokinetic properties with good intestinal absorption, good permeability in Caco-2 system (0.986) and excellent human intestinal absorption (97.48%) suggesting good oral bioavailability (table 3). The physicochemical characteristics indicated moderate lipophilicity (LogP = 2.13) and acceptable solubility (LogS=-3.5) with no Lipinski rule violations, confirming its drug-likeness. Metabolism predictions indicated columbin is a CYP3A4 substrate but does not inhibit major CYP isoforms (CYP3A4, 2D6, 2C9, 1A2), suggesting low drug-drug interaction potential. ADMET predictions indicated no mutagenic potential (AMES negative), low hERG inhibition risk (IC50 >10 μM predicted), and minimal skin sensitization probability (0.12). However, concerning toxicity signals were predicted,

including high DILI probability (0.85) and carcinogenicity potential (0.62), warranting experimental validation (Table 3). The ADMET analysis of columbin (fig. 9) indicates that there is good gastrointestinal absorption because the molecule is located in the white area of the BOILED-Egg plot, which indicates good intestinal permeability. However, it is not located in the yolk region, indicating that columbin is unlikely to cross the blood–brain barrier. The bioavailability radar also supplements the acceptable drug-likeness properties in the optimum physicochemical space.

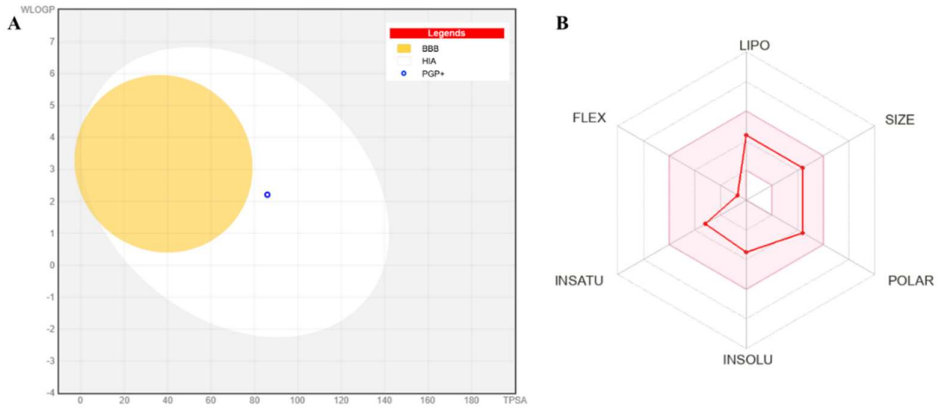

Fig. 9: ---(A) Boiled-egg plot of columbin where gastrointestinal absorption and blood-brain barrier permeability (based on WLOGP, TPSA) are predicted. Columbin is indicated as a blue point. (B) Columbin bioavailability radar plot illustrating some of the key drug-likeness parameters in columbin such as lipophilicity, size, polarity, solubility, saturation and flexibility.

Table 3: --- ADMET properties of columbin predicted using in silico tools, consisting of absorption, distribution, metabolism, excretion, toxicity, and drug-likeness parameters.

Category	Parameter	Value	Category	Parameter	Value
Absorption	GI Absorption	High	**Drug-Likeness**	Lipinski Rule Violations	No Violations
	Caco-2 Permeability (log Papp in 10^{-6} cm/s)	0.986		Molecular Weight (Da)	358.39
	Human Intestinal Absorption (%)	97.485		Log P	2.13
	P-gp Substrate	No		H-bond Donors	1
	P-gp Inhibitor	No		H-bond Acceptors	6
	Water Solubility (log S)	-3.48		TPSA (Å²)	85.97
Distribution	BBB Permeability (log BB)	−0.284		Rotatable Bonds	1
	Volume of Distribution (log L/kg)	0.137		Bioavailability Score	0.55
	Fraction Unbound (Fu)	0.205		Synthetic Accessibility	5.37
Metabolism	CYP1A2 Inhibitor	No	**Toxicity**	AMES Toxicity	No
	CYP3A4 Inhibitor	No		Hepatotoxicity	Yes
	CYP2C9 Inhibitor	No		hERG Inhibition	No
	CYP2D6 Inhibitor	No		LD_{50} (mg/kg)	2.946
	CYP3A4 Substrate	Yes		Skin Sensitization	No
Excretion	Total Body Clearance (log ml/min/kg)	0.79		Drug-Induced Liver Injury (DILI)	0.85
	Renal OCT2 Substrate	Yes		Carcinogenicity	0.62

4. DISCUSSION:

Inflammation is a multi-factorial process with highly interlinked signalling cascades, transcription factors, and immune effectors. While single-target therapies such as TNF-α and IL-6 inhibitors have shown clinical efficacy in inflammatory diseases, resistance to treatments and incomplete responses are prevalent because of redundancy of the pathways and compensatory signalling. These limitations may be overcome by multi-target approaches that can target the condition or disorder on which they are based concomitantly controlling nodes in inflammatory networks that are linked to each other(38). Hence system-level approach is more feasible as it simultaneously interrogates multiple targets. This network pharmacology study predicts multiple targets for inflammation including PI3K–Akt and MAPK cancer signalling pathways (fig. 4). These findings match chronic inflammation processes, where PI3K–Akt activation promotes inflammation and helps immune cells survive and proliferate (39). This multi-pathway action is consistent with previous findings, which have indicated that columbin inhibits nitric oxide and COX-2 generation through many pathways (11).

Docking study found that columbin interacts with all eight proteins, particularly ESR1, MAPK1, and HSP90AA1, which are recognized to play essential roles in inflammatory signalling and immune modulation (40). Gene expression analysis showed only small differences between disease and control groups; however, such modest changes are common for regulatory genes and do not rule out their role in the disease (41). Although most hub genes only presented fold change between 0.6 and 1.8, ROC curve still showed excellent diagnostic value for JAK2 and HSP90AA1, demonstrating that a consistent and directionally changed expression of multiple samples would still be diagnostic for disease states. Each of these genes had individual AUCs that may constitute a useful multi-gene panel, which should be tested in prospectively on independent sets. Besides pathway enrichment analysis, we then further tested whether hub genes correlate with immune cells in actual RA tissue, and the result showed a positive significant correlation between MAPK1 and neutrophils, demonstrating its association with activation of neutrophils. HSP90AA1 has a negative correlation, indicating context-dependent regulation. Resting NK cells showed the strongest negative correlations with PIK3R1 and PTPN11, suggesting participation in NK cell-related activities. The correlations of STAT3, ESR1, and JAK1 with the selected types of immune cells were weaker,

indicating that they have a more limited or context-specific role in this data. Those patterns suggest that various hub genes correspond to various subsets of immune cells. Though these findings do not imply causality, they are supportive evidence of a correlation between patterns of gene expression and immune infiltration in rheumatoid arthritis.

ADMET analysis suggests that columbin possesses favourable pharmacokinetic properties, including high oral absorption, good permeability, and compliance with Lipinski's rule, consistent with previous reports of its systemic availability (Table 3). However, potential hepatotoxicity is predicted, likely due to CYP3A4-mediated bioactivation of its furan ring into reactive intermediates capable of binding to cellular macromolecules (42). Columbin-induced hepatotoxicity is linked to CYP3A-mediated metabolic activation, leading to glutathione depletion, increased ROS production, DNA damage, and subsequent PARP-1 upregulation (43). Although such effects are generally associated with higher doses and may not occur at anti-inflammatory concentrations, they warrant consideration (44). Collectively, these results suggest the therapeutic promise of columbin and emphasize the importance of structural modification to improve its safety characteristics.

There are several limitations that must be considered that may affect the interpretation and applicability of this work to clinical relevance: first, computational prediction of drug targets are associated with a false positive rate, and direct interaction validation by binding assay will be necessary. Second, molecular docking does not represent the dynamic behavior of proteins, and will only predict static binding affinity, and further molecular dynamics will solidify these conclusions. Third, a small size of the validation cohort (GSE55457, n=23 total) was used and large prospective cohort study is necessary to ascertain the diagnostic biomarker potential of predicted targets. Fourth, transciptomic analysis measures only the abundance of mRNA, and not protein abundance or activity. Fifth, hepatotoxicity and DILI predictions require in vivo assessment in animal models and clinical monitoring in trials. Sixth, effectiveness in the anti-inflammatory action of columbin against standard-of-care was not measured which is the most probable clinical utilization.

CONCLUSION:

A systems biology-driven approach was utilized to analyze columbin's molecular targets and anti-inflammatory mechanisms. The data indicate that while being a small molecule, columbin binds favorably to a large number of inflammatory targets, supporting its potential use as a multi-target scaffold for novel drug development. The systems biology methodology used here will pave the way for future network-based natural product discovery. Experimental validation studies, such as binding assays and cell-based studies, are necessary to confirm all predicted targets. Moreover, structure-activity relationship studies are warranted to optimize columbin potency and reduce hepatotoxicity risk. Finally, pre-clinical efficacy studies will be conducted.

CONFLICTS OF INTEREST:

The authors have no competing interests to declare.

REFERENCES:

1. Furman D, Campisi J, Verdin E, Carrera-Bastos P, Targ S, Franceschi C, et al. Chronic inflammation in the etiology of disease across the life span. Nat Med. 2019 Dec;25(12):1822–32. doi:10.1038/s41591-019-0675-0

2. Pahwa R, Goyal A, Jialal I. Chronic Inflammation. In: StatPearls [Internet]. Treasure Island (FL): StatPearls Publishing; 2026 [cited 2026 Apr 15]. Available from: http://www.ncbi.nlm.nih.gov/books/NBK493173/ PubMed PMID: 29630225.

3. Sostres C, Gargallo CJ, Arroyo MT, Lanas A. Adverse effects of non-steroidal anti-inflammatory drugs (NSAIDs, aspirin and coxibs) on upper gastrointestinal tract. Best Pract Res Clin Gastroenterol. 2010 Apr;24(2):121–32. doi:10.1016/j.bpg.2009.11.005 PubMed PMID: 20227026.

4. Buchman AL. Side Effects of Corticosteroid Therapy. J Clin Gastroenterol. 2001 Oct;33(4):289.

5. Puca P, Capobianco I, Coppola G, Di Vincenzo F, Trapani V, Petito V, et al. Cellular and Molecular Determinants of Biologic Drugs Resistance and Therapeutic Failure in Inflammatory Bowel Disease. Int J Mol Sci. 2024 Jan;25(5):2789. doi:10.3390/ijms25052789

6. Murray PJ, Smale ST. Restraint of inflammatory signaling by interdependent strata of negative regulatory pathways. Nat Immunol. 2012 Oct;13(10):916–24. doi:10.1038/ni.2391 PubMed PMID: 22990889; PubMed Central PMCID: PMC4893774.

7. Ge Y jun, Liao Q wen, Xu Y chun, Zhao Q, Wu B li, Ye RD. Anti-inflammatory signaling through G protein-coupled receptors. Acta Pharmacol Sin. 2020 Dec;41(12):1531–8. doi:10.1038/s41401-020-00523-1 PubMed PMID: 33060777; PubMed Central PMCID: PMC7921558.

8. Traditional and clinical use of Tinospora cordifolia, guduchi. Aust J Med Herbal [Internet]. [cited 2026 Apr 15]. Available from: https://search.informit.org/doi/abs/10.3316/informit.408609094525223

9. Fernandes J, Revanasiddappa BC, Ishwarbhat K, Kumar MV, D'Souza L, Alva SS. Synthesis and in-Vitro Anti-Inflammatory Activity of Novel Pyrazoline Derivatives. Res J Pharm Technol. 2017 Jun 28;10(6):1679–82. doi:10.5958/0974-360X.2017.00296.7

10. Jo M, Va R, Jd C, Pj H. Anti-inflammatory activities of the methanol extracts and an isolated furanoditerpene constituent of Sphenocentrum jollyanum

Pierre (Menispermaceae). J Ethnopharmacol. 2006 Mar 8;104(1–2). doi:10.1016/j.jep.2005.08.051 PubMed PMID: 16236477.

11. Ibrahim Abdelwahab S, Syaed Koko W, Mohamed Elhassan Taha M, Mohan S, Achoui M, Ameen Abdulla M, et al. *In vitro* and *in vivo* anti-inflammatory activities of columbin through the inhibition of cycloxygenase-2 and nitric oxide but not the suppression of NF-κB translocation. Eur J Pharmacol. 2012 Mar 5;678(1):61–70. doi:10.1016/j.ejphar.2011.12.024

12. Dash S, Verma S. Phytopharmacological profile of Tinospora cordifolia: An updated review. J Pharmacogn Phytochem. 2026 Mar 9;15(2):47–55. doi:10.22271/phyto.2026.v15.i2a.15770

13. Ibrahim Abdelwahab S, Syaed Koko W, Mohamed Elhassan Taha M, Mohan S, Achoui M, Ameen Abdulla M, et al. In vitro and in vivo anti-inflammatory activities of columbin through the inhibition of cycloxygenase-2 and nitric oxide but not the suppression of NF-κB translocation. Eur J Pharmacol. 2012 Mar 5;678(1–3):61–70. doi:10.1016/j.ejphar.2011.12.024 PubMed PMID: 22227329.

14. National Center for Biotechnology Information (2026). PubChem CID 188289, Columbin. Retrieved April 15, 2026 from https://pubchem.ncbi.nlm.nih.gov/compound/Columbin.

15. Daina A, Michielin O, Zoete V. SwissTargetPrediction: updated data and new features for efficient prediction of protein targets of small molecules. Nucleic Acids Res. 2019 Jul 2;47(W1):W357–64. doi:10.1093/nar/gkz382

16. Yao ZJ, Dong J, Che YJ, Zhu MF, Wen M, Wang NN, et al. TargetNet: a web service for predicting potential drug–target interaction profiling via multi-target SAR models. J Comput Aided Mol Des. 2016 May 1;30(5):413–24. doi:10.1007/s10822-016-9915-2

17. Liu X, Ouyang S, Yu B, Liu Y, Huang K, Gong J, et al. PharmMapper server: a web server for potential drug target identification using pharmacophore mapping approach. Nucleic Acids Res. 2010 Jul;38(Web Server issue):W609-614. doi:10.1093/nar/gkq300 PubMed PMID: 20430828; PubMed Central PMCID: PMC2896160.

18. Gallo K, Goede A, Preissner R, Gohlke BO. SuperPred 3.0: drug classification and target prediction-a machine learning approach. Nucleic Acids Res. 2022 Jul 5;50(W1):W726–31. doi:10.1093/nar/gkac297 PubMed PMID: 35524552; PubMed Central PMCID: PMC9252837.

19. Stelzer G, Rosen N, Plaschkes I, Zimmerman S, Twik M, Fishilevich S, et al. The GeneCards Suite: From Gene Data Mining to Disease Genome Sequence Analyses. Curr Protoc Bioinforma. 2016 Jun 20;54:1.30.1-1.30.33. doi:10.1002/cpbi.5 PubMed PMID: 27322403.

20. Piñero J, Ramírez-Anguita JM, Saüch-Pitarch J, Ronzano F, Centeno E, Sanz F, et al. The DisGeNET knowledge platform for disease genomics: 2019 update. Nucleic Acids Res. 2020 Jan 8;48(D1):D845–55. doi:10.1093/nar/gkz1021 PubMed PMID: 31680165; PubMed Central PMCID: PMC7145631.

21. Woetzel D, Huber R, Kupfer P, Pohlers D, Pfaff M, Driesch D, et al. Identification of rheumatoid arthritis and osteoarthritis patients by transcriptome-based rule set generation. Arthritis Res Ther. 2014 Apr 1;16(2):R84. doi:10.1186/ar4526 PubMed PMID: 24690414; PubMed Central PMCID: PMC4060460.

22. Oliveros JC. Venny. An interactive tool for comparing lists with Venn's diagrams. [Internet]. 2007 2015. Available from: https://bioinfogp.cnb.csic.es/tools/venny/index.html

23. Szklarczyk D, Kirsch R, Koutrouli M, Nastou K, Mehryary F, Hachilif R, et al. The STRING database in 2023: protein-protein association networks and functional enrichment analyses for any sequenced genome of interest. Nucleic Acids Res. 2023 Jan 6;51(D1):D638–46. doi:10.1093/nar/gkac1000 PubMed PMID: 36370105; PubMed Central PMCID: PMC9825434.

24. Franz M, Lopes CT, Huck G, Dong Y, Sumer O, Bader GD. Cytoscape.js: a graph theory library for visualisation and analysis. Bioinformatics. 2016 Jan 15;32(2):309–11. doi:10.1093/bioinformatics/btv557 PubMed PMID: 26415722; PubMed Central PMCID: PMC4708103.

25. Sherman BT, Hao M, Qiu J, Jiao X, Baseler MW, Lane HC, et al. DAVID: a web server for functional enrichment analysis and functional annotation of gene lists (2021 update). Nucleic Acids Res. 2022 Jul 5;50(W1):W216–21. doi:10.1093/nar/gkac194 PubMed PMID: 35325185; PubMed Central PMCID: PMC9252805.

26. O'Boyle NM, Banck M, James CA, Morley C, Vandermeersch T, Hutchison GR. Open Babel: An open chemical toolbox. J Cheminformatics. 2011 Oct 7;3:33. doi:10.1186/1758-2946-3-33 PubMed PMID: 21982300; PubMed Central PMCID: PMC3198950.

27. Zhang M, Jang H, Nussinov R. Structural Features that Distinguish Inactive and Active PI3K Lipid Kinases. J Mol Biol. 2020 Nov 6;432(22):5849–59. doi:10.1016/j.jmb.2020.09.002 PubMed PMID: 32918948; PubMed Central PMCID: PMC8916166.

28. Eberhardt J, Santos-Martins D, Tillack AF, Forli S. AutoDock Vina 1.2.0: New Docking Methods, Expanded Force Field, and Python Bindings. J Chem Inf Model. 2021 Aug 23;61(8):3891–8. doi:10.1021/acs.jcim.1c00203 PubMed PMID: 34278794; PubMed Central PMCID: PMC10683950.

29. Eberhardt J, Santos-Martins D, Tillack AF, Forli S. AutoDock Vina 1.2.0: New Docking Methods,

Expanded Force Field, and Python Bindings. J Chem Inf Model. 2021 Aug 23;61(8):3891–8. doi:10.1021/acs.jcim.1c00203

30. PyMOL | pymol.org [Internet]. [cited 2026 Apr 16]. Available from: https://www.pymol.org/

31. Discovery Studio. San Diego: Dassault Systèmes: BIOVIA, Dassault Systèmes; 2025.

32. Bugnon M, Röhrig UF, Goullieux M, Perez MAS, Daina A, Michielin O, et al. SwissDock 2024: major enhancements for small-molecule docking with Attracting Cavities and AutoDock Vina. Nucleic Acids Res. 2024 Jul 5;52(W1):W324–32. doi:10.1093/nar/gkae300 PubMed PMID: 38686803; PubMed Central PMCID: PMC11223881.

33. Newman AM, Liu CL, Green MR, Gentles AJ, Feng W, Xu Y, et al. Robust enumeration of cell subsets from tissue expression profiles. Nat Methods. 2015 May;12(5):453–7. doi:10.1038/nmeth.3337 PubMed PMID: 25822800; PubMed Central PMCID: PMC4739640.

34. Ritchie ME, Phipson B, Wu D, Hu Y, Law CW, Shi W, et al. limma powers differential expression analyses for RNA-sequencing and microarray studies. Nucleic Acids Res. 2015 Apr 20;43(7):e47. doi:10.1093/nar/gkv007

35. Daina A, Michielin O, Zoete V. SwissADME: a free web tool to evaluate pharmacokinetics, drug-likeness and medicinal chemistry friendliness of small molecules. Sci Rep. 2017 Mar 3;7(1):42717. doi:10.1038/srep42717

36. Pires DEV, Blundell TL, Ascher DB. pkCSM: Predicting Small-Molecule Pharmacokinetic and Toxicity Properties Using Graph-Based Signatures. J Med Chem. 2015 May 14;58(9):4066–72. doi:10.1021/acs.jmedchem.5b00104

37. Banerjee P, Kemmler E, Dunkel M, Preissner R. ProTox 3.0: a webserver for the prediction of toxicity of chemicals. Nucleic Acids Res. 2024 Jul 5;52(W1):W513–20. doi:10.1093/nar/gkae303

38. Medzhitov R. Origin and physiological roles of inflammation. Nature. 2008 Jul 24;454(7203):428–35. doi:10.1038/nature07201 PubMed PMID: 18650913.

39. Fresno M, Alvarez R, Cuesta N. Toll-like receptors, inflammation, metabolism and obesity. Arch Physiol Biochem. 2011 Jul;117(3):151–64. doi:10.3109/13813455.2011.562514 PubMed PMID: 21599616.

40. Kaminska B. MAPK signalling pathways as molecular targets for anti-inflammatory therapy--from molecular mechanisms to therapeutic benefits. Biochim Biophys Acta. 2005 Dec 30;1754(1–2):253–62. doi:10.1016/j.bbapap.2005.08.017 PubMed PMID: 16198162.

41. Domingo J, Minaeva M, Morris JA, Ghatan S, Ziosi M, Sanjana NE, et al. Nonlinear transcriptional responses to gradual modulation of transcription factor dosage. Choi M, editor. eLife. 2026 Jan 14;13:RP100555. doi:10.7554/eLife.100555

42. Pei J, Xiao W, Zhu D, Ji X, Shi L, Deng X. Cytochrome P450 Enzyme-Mediated Bioactivation as an Underlying Mechanism of Columbin-Induced Hepatotoxicity. Chem Res Toxicol. 2020 Apr 20;33(4):940–7. doi:10.1021/acs.chemrestox.9b00486

43. Liao Y, Wang X, Ran G, Zhang S, Wu C, Tan R, et al. DNA damage and up-regulation of PARP-1 induced by columbin in vitro and in vivo. Toxicol Lett. 2023 Apr 15;379:20–34. doi:10.1016/j.toxlet.2023.03.003 PubMed PMID: 36905973.

44. Moody JO, Robert VA, Connolly JD, Houghton PJ. Anti-inflammatory activities of the methanol extracts and an isolated furanoditerpene constituent of *Sphenocentrum jollyanum* Pierre (Menispermaceae). J Ethnopharmacol. 2006 Mar 8;104(1):87–91. doi:10.1016/j.jep.2005.08.051